MDPI

Article

Optimization of Ratio and Hydration Mechanism of Titanium-Extracted Residual Slag-Based Filling Cementitious Materials

Jielin Li [1,*], Ao Li [1], Jianzhang Hao [2], Jiye Xu [3], Ming Li [2] and Keping Zhou [1]

1   School of Resources and Safety Engineering, Central South University, Changsha 410017, China; 215511041@csu.edu.cn (A.L.); kpzhou@vip.163.com (K.Z.)
2   Ansteel Research Institute of Vanadium & Titanium, Pangang Group Research Institute Co., Ltd., Panzhihua 617067, China; hjz980809@126.com (J.H.); liming00929@163.com (M.L.)
3   Design and Research Institute, Pangang Group Mining Co., Ltd., Panzhihua 617067, China; 18782345347@163.com
*   Correspondence: lijielin@163.com; Tel.: +86-13873137080

Abstract: Using metallurgical solid waste Titanium-extracted Residual Slag (TRS) as mine-filling cementitious material is crucial to reduce the filling cost and promote the utilization of solid waste resources. In this paper, taking the strength of the backfill at different curing ages as the response target, the Design-expert mixing design was used to optimize the proportioning experiment of titanium-extracted residual slag, titanium gypsum, silicate cement, and total tailings, to analyze the interactions and influences of the materials on the strength of the backfill, and to analyze the hydration mechanism of the titanium-extracted residual slag-based filling cementitious materials under the optimal proportioning. The results show that: (1) the order of the sensitivity of each component to the strength of backfill is: composite activator > cement > titanium gypsum > titanium-extracted residual slag, and there are different degrees of interaction between them; (2) the optimal ratio of titanium-extracted residual slag-based filling cementitious materials is TRS:titanium gypsum:cement:composite activator = 55:25:17:3; (3) early strength formation of backfill is mainly related to its hydration products ettringite and C-S-H, the rapid nucleation and cross-growth of ettringite in the early stage forms an effective physical filling effect, which is the main reason for the formation of high early strength, and the later strength of backfill benefited from the continuous accumulation of C-S-H encapsulation and bonding, which further densified its internal structure; (4) the use of titanium-extracted residual slag-based filling cementitious materials contributes to safe, green, and economic mining.

Keywords: titanium-extracted residual slag; response surface analysis; mixing experiment; solid waste utilization; ratio optimization; hydration mechanism

1. Introduction

The filling mining method has gradually become the most widely used mining method in the modern mining industry [1–3]. As the cementing agent of mine filling, the filling cementing material directly affects the backfill's performance and the filling material's cost. Currently, the most widely used cementing materials in mines are still various types of cement, and the material cost of cement in the filling process accounts for 60%–80% [4]. Therefore, the study of cheap cementing materials suitable for mine filling is in line with the development trend of mine resource utilization and economy [5]. The application of waste slag from various metallurgical fields and thermal power plants to develop new cementing materials is a hot research topic at present [6–10], which has important practical significance for enterprises to reduce costs, increase efficiency, and improve economic benefits.

Titanium-extracted Residual Slag (TRS) is the residue remaining after the titanium element is converted into an independent physical phase and extracted away from the high-titanium blast furnace slag through high-temperature carbonization and low-temperature

chlorination process [11]. The resource utilization of TRS is the final problem of extracting valuable elements from titanium-containing blast-furnace slag. The continuous accumulation of titanium tailings has caused great pressure on the whole industrial chain. Currently, TRS is mainly used as raw materials to make microcrystalline casting stone, hollow brick blocks, corundum-based castable binders, ceramic particles, glass ceramics, free-burning brick, or steamed brick [12]. At the same time, the TRS has a certain hydration-gelling activity. After grinding, the hydration activity of the TRS can be significantly improved and can be used as a substitute for filling cement, with a maximum replacement amount of 50% [13]. Due to the research mentioned above on the resource utilization of TRS, there are still problems of low economic benefits and small processing capacity. Some scholars have begun to pay attention to the development of cementing materials based on titanium tailings extraction and have applied them to mine filling [14]. Therefore, it is of obvious practical significance to explore and develop the titanium-extracted residual slag-based filling cementitious materials based on the activity characteristics of TRS for the resource utilization of TRS.

In previous studies, many researchers have conducted a lot of research on metallurgical solid waste base filling cementing material. Liao et al. [15] have conducted a whole system study on the cementing property, alkali excitation property, and hydration mechanism of the yellow phosphorus slag, and developed a kind of filling cementing material with wider prospects and cheaper. Ren et al. [16] prepared steel slag and other industrial solid wastes into mine filling materials, explored the mechanical activation law of steel slag mud, and provided a theoretical basis for the resource utilization of steel slag mud. Zhang et al. [17] used blast furnace slag as raw material to form a binder in slag material by adding cement clinker, gypsum, and activator with different contents and discussed the cementing mechanism of slag cementing material in mine backfill according to the strength and capacity law of backfill body. Lan et al. [18] developed a new controllable low-strength filling material for copper slag in an African mine by using mechanical activation and alkali excitation so that its filling cost was comparable to that of cement. Zhang et al. [19] used coal gangue as crude material, fly ash, desulfurized gypsum, gasification slag, furnace bottom slag as fine material, and cement as a gelling agent. The uniaxial compressive strength and seepage rate of coal-based solid waste cemented backfill were analyzed, and the factors affecting the development of mechanical properties and strength were analyzed. Multiple generalized linear models of strength and seepage rate were established, and the optimal ratio of filling materials was determined. El-Didamony et al. [20] prepared cement-based granulated slag and waste marble powder composite material to partially replace Portland cement by up to 20% and studied its mechanical properties and hydration mechanism. The current research primarily focuses on common solid waste materials such as steel slag. Utilizing conventional test methods for grinding and alkaline excitation materials to enhance the activity of cementified materials can result in a filling cementified material with relatively excellent properties. However, the treatment of solid waste remains largely uniform, leading to high economic costs and overlooking the differences in material distribution across various regions. As a solid waste in the Panzhihua area, the TRS holds significant potential value, yet there is limited research on it at present. To address the issue of resource utilization, it mainly utilizes locally available solid waste materials and activators to explore its properties, which is crucial for improving the economic viability of materials and regional compatibility.

In this paper, the ratio experiments of TRS, titanium gypsum, Portland cement, and composite activator were designed with the strength of different curing ages as the response target by fixing the Cement-sand ratio or Water-binder ratio. Design-Expert software (Design-Expert 12.0) was used to analyze the experimental results, and the corresponding strength regression model was established. The interaction and influence effect of each component on the strength of the backfill were analyzed, and the optimal ratio of the titanium-extracted residual slag-based filling cementitious materials was obtained. On this basis, the hydration mechanism of the titanium-extracted residual slag-based filling

cementitious materials was further explored under the optimal ratio condition. The mining and metallurgical industry is highly energy-intensive, and the total carbon emission control pressure is huge, which can be effectively solved through the deep integration of the upstream and downstream low-carbon innovation value chain and the transformation of traditional industries. Therefore, the development of titanium tailings as mine filling cementing material scheme can simultaneously treat industrial solid waste for upstream and downstream industries of Pangang Group, reduce filling costs, create economic benefits, and is also an effective way to achieve the goal of "carbon peaking and carbon neutrality" sustainable development.

2. Experimental Content

2.1. Experimental Materials

To obtain more practical and economical composite cementitious materials, The main raw materials of the experiment include typical solid waste Titanium-extracted Residual Slag (TRS), titanium gypsum (TG), and iron-based total tailings (IFT) from the Panzhihua City, Sichuan Province in China, and Portland cement (P.O 42.5R) and composite activator are used to activate TRS. The appearance of the main experimental materials is shown in Figure 1, and the chemical composition analysis is shown in Table 1. To improve the hydration activity of the gelling material, the TRS and TG were dried and then ground. The comparison of particle sizes of each material is shown in Figure 2.
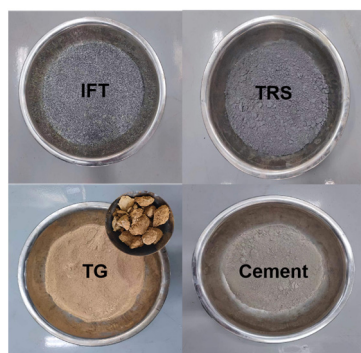
Figure 1. Appearance of main experimental materials.
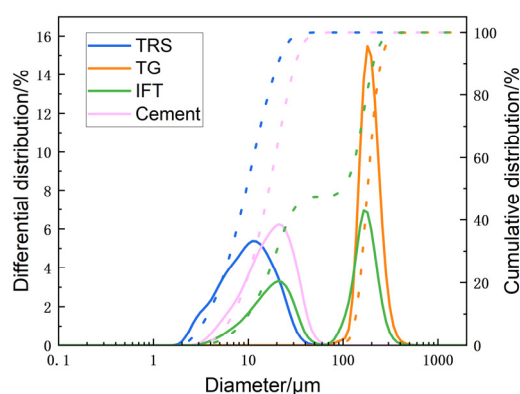
Figure 2. Particle size analysis graph.

- Titanium-extracted Residual Slag

The TRS is taken from the smelting demonstration line of a group in the Panzhihua city. The TRS is a gray-gray brown fine powdery material, which easily hardens and absorbs moisture, and the loose bulk weight is 0.851 g/cm^3. The average particle size of the TRS is 11.91 μm, the particle size less than 3.83 μm accounted for 10%, the particle size less than 10.08 μm accounted for 50%, and the particle size less than

22.64 μm accounted for 90%, which belongs to the ultrafine particle grade material. According to the data in Table 1, the alkalinity coefficient of the TRS is calculated as Mo = (ωCaO + ωMgO)/(ωSiO$_2$ + ωAl$_2$O$_3$) = 0.91 < 1. It can be seen that the TRS is acidic furnace slag.

- Titanium gypsum

Titanium gypsum is taken from a high-tech industrial park in Panzhihua city, the main component of titanium gypsum is calcium sulfate dihydrate, the whole is the yellowish-brown block, the original water content is about 33%, yellow after drying, the average particle size after grinding 188.45 μm, less than 249.92 μm particle size accounts for more than 90%. Titanium gypsum is simple in composition, and the main oxide components are SO$_3$, CaO, and Fe$_2$O$_3$.

- Iron base total tailings

Total tailing was taken from an iron mine in Panzhihua City. It was an uneven grayish-white powdery solid with an original water content of about 15%. After drying, the measured specific gravity was 3.3, the loose bulk weight was 1.695 g/cm^3, and the porosity was 47.93%. The grading of total tailing was discontinuous, and the total tailing with a particle size less than 30.00 μm accounted for about 39.92%. The main components of total tailings are SiO$_2$, Al$_2$O$_3$, and CaO (63.39% in total), which is conducive to the strength development of the backfill.

- Portland cement

Portland cement grade P.O 42.5R, specific surface area > 350 m^2/kg.

- Composite activator

Composite activator consists of quicklime, calcium formate, and sodium sulfate in a specific proportion, and each material is analytically pure grade.

Table 1. Results of chemical composition analysis.

ω%	CaO	MgO	MnO	SiO$_2$	TiO$_2$	Al$_2$O$_3$	SO$_3$	Fe$_2$O$_3$	Cl	TiC	Na$_2$O	V$_2$O$_5$
TBS	26.52	8.78	0.71	25.3	5.98	13.15	0.98	—	3.28	2.75	—	—
IFT	12.7	9.2	0.181	37.49	4.355	13.2	1.01	13.24	0.026	—	0.98	—
TG	30.66	5.21	0.179	1.83	1.44	0.68	36.53	17.78	—	—	—	0.033

2.2. Mixing Experimental Design

Mixing design is a method of designing formulation experiments, the test index only depends on the proportion of each component and has nothing to do with the total amount of mixing. The mixing design differs from the orthogonal experiment in its purpose and experimental design principles. The focus of the mixing design is to optimize the ratio of each component in the mixture. In contrast, the orthogonal design considers multi-factor interaction comprehensively and aims to improve experimental efficiency. In this test, we aim to obtain a better composition ratio of TRS gelling material, hence the selection of mixing design. In this experiment, The A-optimal design was selected, in which blocks, additional models, lack of fit, and centroid requested during repetition and construction were added according to the corresponding process, which would improve the applicability and robustness of the model. Through the test, the empirical model of the relationship between the test index and each component of the mix can be established, and the test index can be optimized proportional to the value of each component.

According to the requirements of the cemented filling process of the filling mining method and the results of the slump test, the experimental design was carried out by using the Mixture module of the Design-Expert software to explore the factors influencing the strength of the backfill and the range of strength. Four influencing factors, namely, TRS, titanium gypsum, silicate cement, and composite exciter (denoted by A, B, C, and D,

respectively), were selected as independent variables, and the compressive strengths of the backfill at 3d, 7d and 28d (denoted by S1, S2 and S3, respectively) were taken as the response values to investigate the effects of the variables and their interactions on the strengths of the backfill. According to pre-experimental results, the values of the variables were set as follows: TRS + cement + titanium gypsum + composite exciter = 100%, TRS range 50%–70%, titanium gypsum range 10%–25%, cement range 0%–20%, and composite exciter range 0%–10%.

2.3. Experimental Methodology

2.3.1. Mixing Experimental Methods

Referring to "Granulated Blast Furnace Slag Powder Used in Cement, Mortar and Concrete" (GB/T18046-2017) [21], the relevant experimental parameters are: ash-sand ratio of 1:3, the water-cement ratio of 2:3 (ash refers to the mixture of TRS slag, titanium gypsum, silicate cement and composite excitant, and sand refers to the whole tailing sand). The test program will mention TRS slag, titanium gypsum, silicate cement, and composite excitant according to the design proportion of mixing and then mixed with water, the use of mixer mixing loaded into $40 \times 40 \times 160$ mm triple flexural compression mold, vibration, and adding material after 2 h of static scraping treatment, 24 h after demolding, demolded test piece into a constant temperature and humidity maintenance box (temperature (20 ± 1) °C, humidity $\geq 90\%$), and the maintenance to the specified age. Then, the test piece is placed into a constant temperature and humidity maintenance box (temperature (20 ± 1) °C, humidity $\geq 90\%$). Maintenance takes place according to the specified age for compressive tests.

2.3.2. Methods of Micro-Mechanism Analysis

Raw materials, mixed cementitious materials, and filled body samples were analyzed and tested. The XRD test was carried out using a Dutch Parnack Empyrean X-ray diffractometer (XRD) (Carl Zeiss (Shanghai) Management Co., Ltd., Shanghai, China) for the physical phase detection of the 200-mesh sieve substrate after milling, with a scanning speed of $1°$ min^{-1}, and a scanning range of $5°$ to $70°$. The XRD test can detect the mineral components contained in the samples. Before the test, the bulk samples were dried and ground into powder, and the powdered samples were poured into the center of the sample tray and covered with a clean glass sheet, and then the titanium lifting tailings, the whole tailings sand, and the collodion materials of each hydration age were tested. Sigema 500 scanning electron microscope was used to observe the microscopic morphology of some materials as well as the test pieces. Before the test, the granular samples were dried and then glued to the conductive adhesive for gold spraying. In the SEM test parameters, the accelerating voltages were 5 kV and 10 kV, the magnification was 5000–500,000 times, and the working distances were 7–9 mm. The technology roadmap is shown in Figure 3.
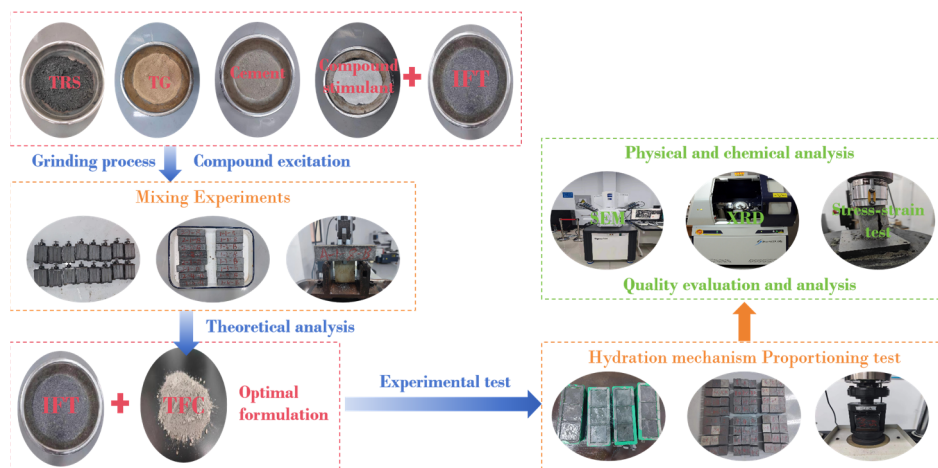

Figure 3. Pilot technology roadmap.

3. Response Surface Analysis of Mixing Experiment Results

3.1. Strength Regression Model Analysis for Different Maintenance Ages

The results of the mixing experiment are shown in Table 2. It can be seen that the compressive strength of the samples of each experimental group increases with the increase in curing age. The minimum strength of each age group is 0.30 MPa, 0.40 MPa, and 6.70 MPa, and the maximum strength is 11.27 MPa, 18.35 MPa, and 40.57 MPa, respectively. The difference in compressive strength among all groups is obvious. It indicates that each component of the cementitious material filled with TRS has a great influence on the strength of total tailings consolidated backfill at different ages. Design-Expert software was used to multivariate nonlinear fit the 24 groups of experimental data in Table 3, and the response model of the relationship between the compressive strength of the backfill at different curing ages and the content of TRS, TG, cement, and composite motivator was established, as shown in (1)–(3). The model is set according to the fitting characteristics. After removing the non-significant items in the simulation, the regression model equation of strength (S) can be expressed as: (A: TRS; B: TG; C: Cement; D: composite activator):

- Curing compressive strength for 3d, $R^2 = 0.944$

$$S_1 = -5.91A - 155.51B + 4.07C - 818.77D + 212.23AB + 1089.28AD + 1062.21BD + 435.84BC + 539.05CD \quad (1)$$

- Curing compressive strength for, $R^2 = 0.978$

$$S_2 = -61.40A + 60.59B - 1161.69C - 3502.58D + 1712.23AC + 4391.467AD + 1621.09BC + 4427.97BD \\ + 19206.31CD - 19574.11ACD - 29822.71BCD \quad (2)$$

- Curing compressive strength for 28d, $R^2 = 0.977$

$$S_3 = -109.35A - 53.71B + 177.85C - 1433.27D + 457.00AB + 260.88AC + 2707.05AD - 280.89BC + 642.39BD \quad (3)$$

As can be seen from the above equation,

1. The cement mainly promotes the growth of 3d strength and 28d strength, and TG has a positive effect on the growth of 7d strength;
2. The strength of the whole backfill mainly depends on the combination of various materials;
3. The 3d strength and 28d strength of backfill are mainly affected by TRS and composite activators, and the composite activation of TRS has a significant impact on the early and late strength of backfill;
4. The 7d strength of the backfill is affected by the composite effect of three kinds of materials except TRS, which will significantly reduce the 7d strength of the backfill.

According to the experimental results, ANOVA was used to test the growth relationship of the above uniaxial compressive strength. The ANOVA method is also used to estimate the influence of parameter uncertainty on response variability. ANOVA investigates sources of sample uncertainty or error by estimating the mean of squares between and within groups of different groups. The ANOVA of the reduced quadratic model is shown in Table 3. As can be seen from Table 3, the minimum F value of the model is 31.98, which is greater than F0.05 (3,9) = 3.86, indicating that the model is significant and statistically significant, and can better reflect the relationship between the compressive strength of backfill and various influencing factors.

Model *p* value less than 0.0001 indicates significance, and residual difference greater than 0.05 is not significant, indicating the strength of backfill at various curing ages. Its correlation coefficient R^2 ranges from 0.944 to 0.978, all of which are close to 1, indicating that the coefficient of variation of the model is small and the model confidence is high, indicating that the analysis conclusion of the influence of various factors on the strength is credible. Figure 4 is the normal residual diagram of each model, and the distribution of each point is close to a straight line, which further indicates that the model is well-fitted and can well characterize the relationship between the response value backfill strength and the influence factor.

Table 2. Experimental results of mixed design.

Number	Component Proportion/%				Compressive Strength/MPa		
	A	B	C	D	3d	7d	28d
1	0.70	0.13	0.17	0.00	5.1	6.98	14.07
2	0.70	0.17	0.09	0.05	8.33	9.85	18.70
3	0.70	0.25	0.00	0.05	5.43	7.80	24.30
4	0.51	0.25	0.14	0.10	8.68	10.10	32.00
5	0.62	0.20	0.12	0.06	9.87	14.48	33.63
6	0.64	0.21	0.05	0.10	9.20	12.10	36.50
7	0.70	0.13	0.17	0.00	5.47	6.85	13.93
8	0.68	0.25	0.07	0.00	0.33	0.53	6.70
9	0.57	0.16	0.20	0.06	11.13	14.10	40.57
10	0.50	0.25	0.20	0.05	11.27	13.08	39.70
11	0.58	0.22	0.20	0.00	10.50	16.25	36.60
12	0.68	0.10	0.12	0.10	10.57	12.38	39.40
13	0.65	0.18	0.12	0.05	12.20	15.35	33.77
14	0.58	0.22	0.20	0.00	8.67	14.55	35.53
15	0.68	0.10	0.12	0.10	10.07	12.63	38.70
16	0.68	0.25	0.07	0.00	0.30	0.40	8.90
17	0.56	0.25	0.15	0.04	10.17	18.35	37.87
18	0.51	0.19	0.20	0.10	10.43	13.38	39.37
19	0.51	0.19	0.20	0.10	10.17	13.23	36.23
20	0.62	0.20	0.12	0.06	11.03	15.70	35.63
21	0.70	0.20	0.00	0.10	9.30	14.50	34.77
22	0.57	0.25	0.08	0.10	8.77	13.40	38.17
23	0.65	0.10	0.20	0.05	8.60	13.40	34.37
24	0.62	0.13	0.15	0.10	9.07	13.08	39.80

Table 3. Reduced results of quadratic model ANOVA.

Source	Sum of Squares			df	Mean Square			F-Value			*p*-Value		
	S_1	S_2	S_3		S_1	S_2	S_3	S_1	S_2	S_3	S_1	S_2	S_3
Model	209.23	461.19	2534.66	13	16.09	35.47	194.97	19.28	64.17	42.75	<0.0001	<0.0001	<0.0001
Line mixture	116.11	174.44	1671.91	3	38.70	58.14	557.30	46.38	105.18	122.20	<0.0001	<0.0001	<0.0001
AB	2.04	2.00	4.71	1	2.04	2.00	4.71	2.45	3.63	1.03	0.148	0.085	0.333
AC	6.50	33.40	20.64	1	6.50	33.40	20.64	7.79	60.41	4.52	0.019	<0.0001	0.059
AD	2.28	14.96	10.14	1	2.28	14.96	10.14	2.73	27.06	2.22	0.129	0.0003	0.166
BC	5.14	17.91	7.10	1	5.14	17.91	7.10	6.16	32.41	1.55	0.032	0.0002	0.240
BD	3.66	9.16	5.60	1	3.66	9.16	5.60	4.39	16.57	1.22	0.062	0.002	0.293
CD	4.23	29.36	9.14	1	4.23	29.36	9.14	5.08	53.12	2.00	0.047	<0.0001	0.187
ABC	2.10	4.07	1.66	1	2.10	4.07	1.66	2.52	7.36	0.36	0.143	0.021	0.558
ABD	1.10	1.21	4.45	1	1.10	1.21	4.45	1.32	2.19	0.97	0.276	0.169	0.346
ACD	2.57	29.39	8.52	1	2.57	29.39	8.52	3.09	53.16	1.86	0.109	<0.0001	0.201
BCD	2.82	19.20	8.78	1	2.82	19.20	8.78	3.38	34.73	1.92	0.095	0.0001	0.195
Residual	8.34	5.52	45.60	10	0.83	0.55	4.56						
Lack of Fit	6.25	3.28	33.64	4	1.56	0.822	8.41	4.48	2.19	4.22	0.0511	0.186	0.057
Pure Error	2.09	2.24	11.95	6	0.34	0.37	1.99		64.17	42.75			
Cor Total	217.58	466.72	2580.26	23									

Figure 4. Normal plot of residuals (**a**) curing age at 3 days; (**b**) curing age at 7 days; (**c**) curing age at 28 days.

3.2. Influence and Effect of Various Factors of Filling Cementing Material

3.2.1. Influence Analysis of Factors

It can be seen from the fitting results that cement partially promotes the 3d strength of the backfill, which is beneficial to the 3d strength of the backfill, but other factors acting alone will reduce the strength of the backfill. Therefore, the sensitivity of the 3d strength of the backfill is ranked in the following order: composite activator > TG > TRS > cement; For the 7d strength of the backfill, TG enhanced the strength of the backfill, while other factors acting alone reduced the strength of the backfill, and the sensitivity to the 7d strength of the backfill was in the following order: composite activator > cement > TRS > TG. For the 28d strength of backfill, cement plays a role in enhancing it, but when other factors act alone, the strength of backfill is reduced, and the sensitivity to the 28d strength of backfill is as follows: composite activator > cement > TRS > TG.

On the whole, the effect of a single factor on the strength of the backfill is a side effect, and the formation of the strength of the backfill mainly depends on the composite excitation of the TRS.

3.2.2. Analysis of the Effects of Each Factor

Some characteristic 3D response surfaces reflecting 3d, 7d, and 28d intensity were analyzed successively. As shown in Figure 5a, when the cement content is constant, the 3d strength of backfill is affected by the composite of the other three factors and mainly increases significantly with the decrease in the TRS. Secondly, the strength of the backfill initially increases and then decreases as the content of the composite activator increases. The impact of TG on strength is relatively minor, indicating that early strength primarily depends on the amount of activated TRS. Under the condition of 10% cement content, when the middle value of the activator, the maximum value of TG, and the minimum value of TRS, it is expected that there will be a peak 3d strength. Figure 5b illustrates that when the activator content is 0.05, there is a steep increase in strength. With higher TRS values, TG has a greater influence than cement does. Conversely, with lower TRS values, increasing TG and cement content leads to increased backfill strength due to their combined effect.
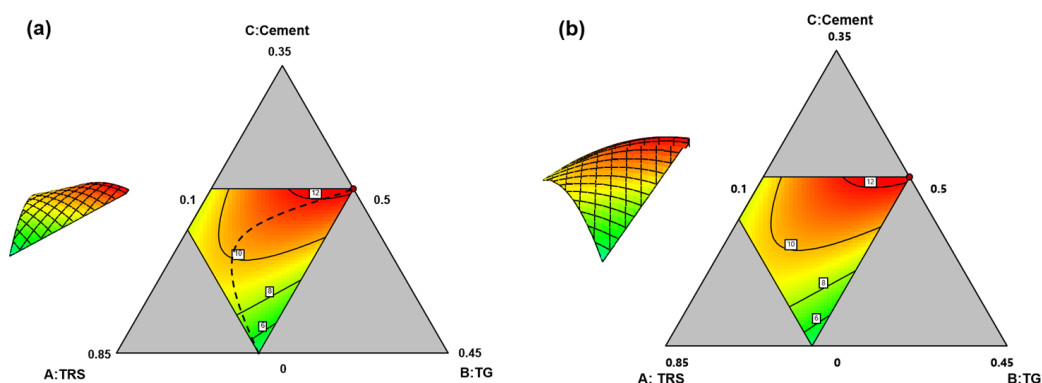
Figure 5. Curing age 3d (**a**) Cement = 0.1; (**b**) Activator = 0.05.

The 7d strength change of backfill is shown in Figure 6. Under the condition of 0.1 dosages of cement when the content of TRS was moderate, both TG and activator showed obvious excitability to the 7d strength of backfill, and when the proportion of activator was maximum, they showed better strength characteristics, and the overall effect of activator was greater than that of TG. It can be seen from Figure 6b that when the content of the activator is 0.1, the strength of the 7d backfill body shows the same two peaks, indicating that TG plays an obvious role in the strength formation process at this stage, which is close to the effect of cement and activator.
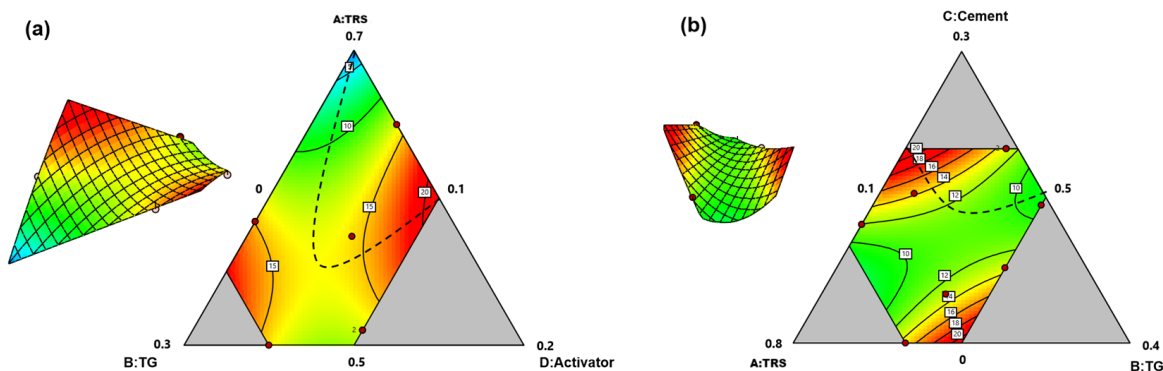
Figure 6. Curing age 7d (**a**) Cement = 0.1; (**b**) Activator = 0.1.

The strength change in backfill at 28d is shown in Figure 7. When the cement content is 0.2, both TG and composite activator have a significant increase in strength in the later stage. The lower the dosage of TRS, the higher the strength in the later stage. When the content of the activator is 0.05, the strength of the backfill increases with the reduction of TRS, and the higher the TG and cement, the higher the strength of the backfill. On the whole, in the whole mixed material system, TG, cement, and composite activator can stimulate the hydration reaction of TRS in each age, to improve the overall strength of backfill. A certain amount of TG can significantly improve the strength of the backfill at the early stage, significantly reduce the cost of the titanium-extracted residual slag-based filling cementitious materials, and improve its application scenarios and promotion value.
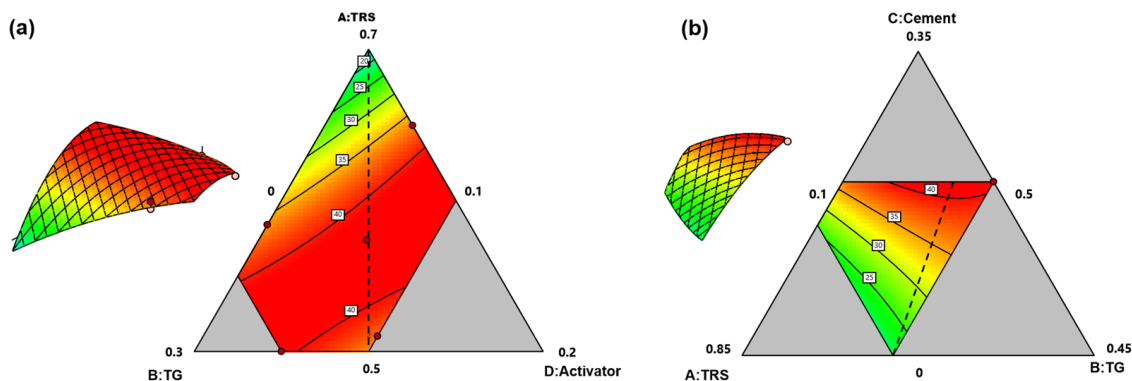
Figure 7. Curing age 28d (**a**) Cement = 0.2; (**b**) Activator = 0.05.

3.3. The Titanium-Extracted Residual Slag-Based Filling Cementitious Materials Ratio Optimization and Evaluation

3.3.1. Ratio Optimization

As shown in Table 4, The optimal ratio was designed by Design-Expert software, and under the condition that the content of cement and composite activator was as low as possible, the ratio of each material was comprehensively adjusted to make the strength response value of each age backfill reach the highest as possible. The regression model was used to optimize the ratio of TRS, TG, cement, and composite activator. The test results show that the optimal ratio of titanium-extracted residual slag-based filling cementitious material is TRS:TG:cement:composite activator = 55:25:17:3. The optimal ratio strength values predicted by the model for each age are 10.24 MPa, 18.35 MPa, and 44.22 MPa, respectively, and the results verified by laboratory experiments are 10.73 MPa, 17.92 MPa, and 41.20 MPa. The deviation between the overall result and the predicted result is within 9.67%, which proves the accuracy of the prediction model.

Table 4. Matching optimization test.

Order	Optimized Combination/%				Predicted/MPa			Actual/MPa			Predicted Deviations/%		
	A	B	C	D	3d	7d	28d	3d	7d	28d	3d	7d	28d
1	0.55	0.25	0.17	0.03	10.24	18.35	44.22	10.73	17.92	41.20	4.79	2.34	6.83
2	0.65	0.25	0	0.1	8.55	10.34	39.45	9.25	11.34	38.63	8.19	9.67	2.08
3	0.57	0.25	0.12	0	10.32	14.83	40.03	10.23	14.27	38.80	0.87	3.78	3.07

3.3.2. Filling Performance Evaluation of Cementitious Materials

- Water absorption

According to the optimized ratio, the appearance of the cement material filled with titanium tailings is shown in Figure 8, which is a grayish-white powder solid with a loose density of 0.89 g/cm^3 and a specific surface area of 0.037 m^2/cm^3. As shown in Figure 9, Compared with TRS, which is a very absorbent raw material, the overall water absorption

of the composite cementing material is reduced by about 50%, which is conducive to the transportation and preservation of cementing material.
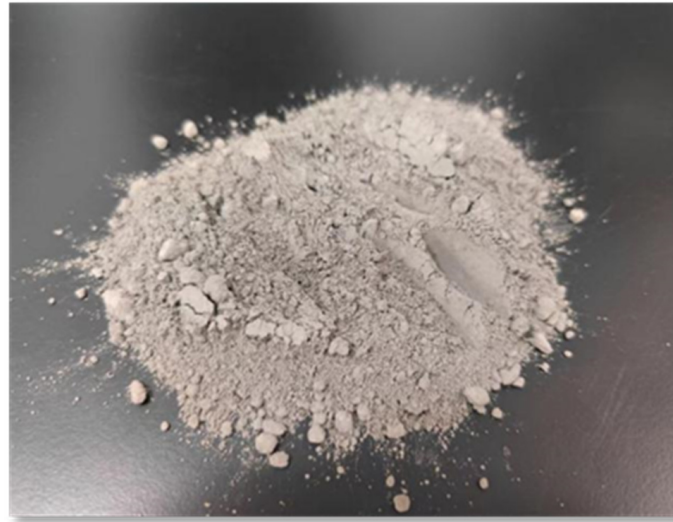

Figure 8. The titanium-extracted residual slag-based filling cementitious materials.
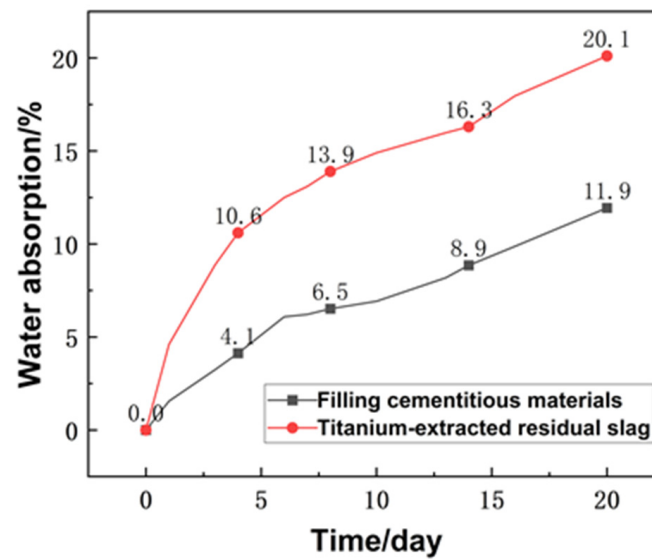

Figure 9. Water absorption performance.

Concerning "GB/T51450-2022 Technical Standard for Metal and Non-metal Mine Filling Engineering" [22], the ratio of lime to sand was set at 1:4, the mass concentration of slurry was 72%, and the strength of the backfill of 3d, 7d, 14d, and 28d were tested concerning the pure cement slurry. The comparison results are shown in Figure 10. The results show that the 3d, 7d, and 14d strength of the backfill prepared by using the optimal ratio of the titanium-extracted residual slag-based filling cementitious materials can reach 76%, 87%, and 96% of the strength of cement sample, and the strength of 28d can exceed the strength of cement test block, reaching 4.83 MPa. The strength of the backfill increased rapidly within 7 days, but the growth rate slowed down after 7 days, indicating that the new cementitious material has obvious early strength characteristics, which is conducive to shortening the stope filling and curing time, increasing the number of mining cycles within the same time, and significantly improving the production capacity of the stope.
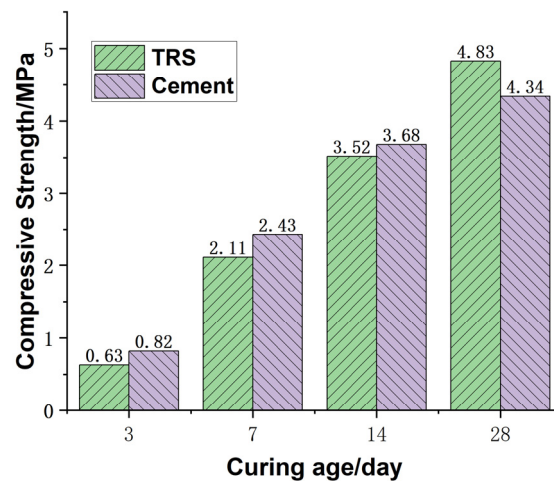
Figure 10. Comparison of strength of backfill.

4. Analysis of the Microscopic Hydration Mechanism of TRS Slag-Based Composite Cementitious Materials

4.1. Material Activity Mechanism Analysis

There are many factors affecting the activity of slag-like materials, mainly with the fineness of the slag itself, the chemical composition, and the content and structure of the vitreous humor are closely related. The internal mineral phase of TRS after grinding will produce defects and lattice distortion, which can increase the contact area with water, which is conducive to enhancing the degree of hydration and improving the hydration rate [23–25]. The TRS is formed by rapid cooling after titanium removal from high titanium blast furnace slag. This process will form a large number of glass phases inside the TRS. Using an X-ray diffractometer (XRD) for TRS physical phase detection, as can be seen in Figure 11, it can be found that the TRS crystallinity is not obvious, and there are obvious bulging peaks reflecting its internal rich amorphous glassy structure, which has a better hydration reaction activity [26,27].
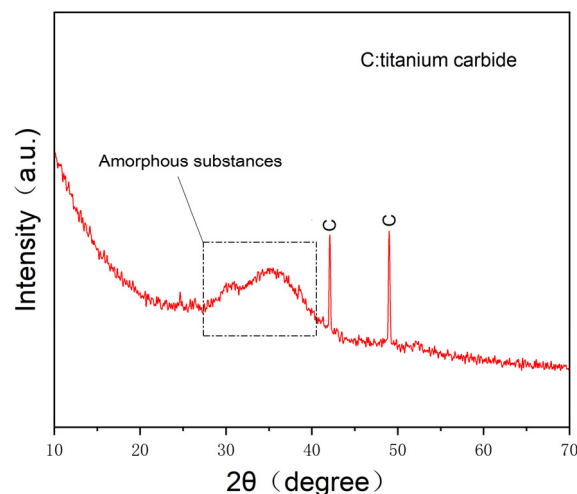
Figure 11. The XRD test of TRS.

The particle size analysis of the cementitious materials in Figure 12 reveals an average particle size of 193.08 microns, with a relatively concentrated overall distribution on the particle size distribution graph. This demonstrates excellent particle size grading of the mixed material and even mixing of all materials, both of which play a crucial role in the physical properties and hydration reaction of the material.
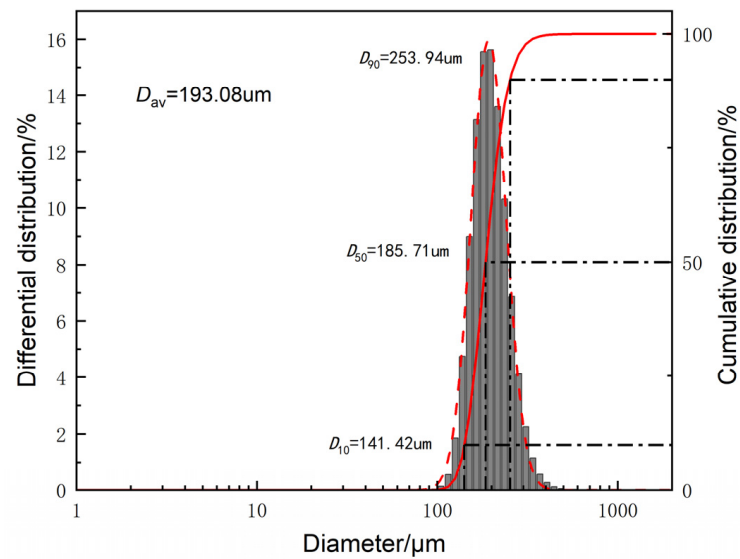
Figure 12. The particle size analysis of the cementitious materials.

The titanium-extracted residual slag-based filling cementitious material was subjected to an SEM test, and it can be seen from Figure 13 that the particle size of TG is the largest, the particle size of cement and TRS is close to that of TG, and in a large number of irregular TG interstices are filled with TRS and cement which are combined into a small group. The three materials are tightly combined and do not react, and the surface of the composite cementitious material is uneven, which is favorable for the combination of the reaction with the water.
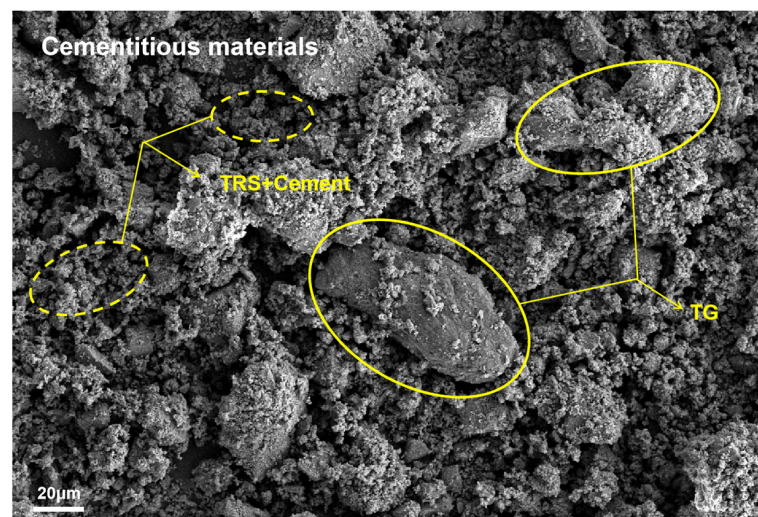
Figure 13. Microscopic morphology of cementitious materials.

4.2. The Titanium-Extracted Residual Slag-Based Filling Cementitious Materials Hydration Mechanism Analysis

4.2.1. Hydration Products and Hydration Reactions

Figure 14 shows the XRD pattern of the clean paste sample of the cementified material at different ages. As can be seen from Figure 14, the hydration products of the net paste of the cementing material at different ages are the same, only the diffraction peak strength is different. The main mineral phases are ettringite, calcium carbonate, potassium feldspar, calcium silicate hydrate generated by the reaction, and a small amount of calcium aluminate hydrate.
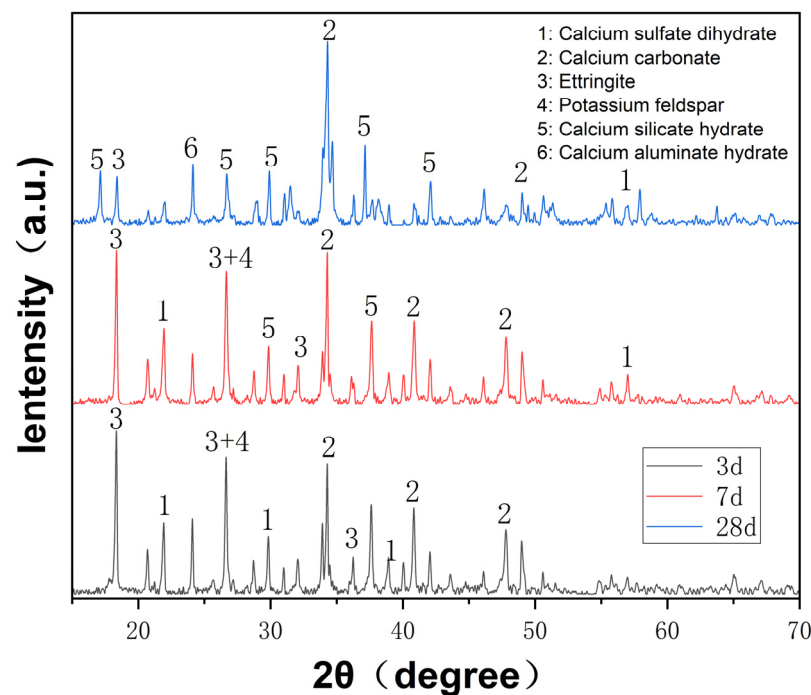
Figure 14. Hydration XRD diagram of net slurry samples of composite cementitious materials.

The main chemical products at all ages were ettringite and C-S-H gels. At the curing age of 3d, some ettringite and hydrated gel were generated, then the generation of ettringite increased rapidly, and a large amount of calcite and hydrated calcium silicate appeared at the curing age of 7d, and thereafter until 28d, there was little change in the intensity of the diffraction peaks, and the total amount of each substance increased gradually, and the growth rate was slowed down. In the whole process of the hydration reaction, calcium sulfate dihydrate, and calcium sulfate hemihydrate in TG also participated in the reaction, generating ettringite and calcium carbonate, which promoted strength growth [28].

The early hydration activity of TRS was dramatically increased after it was modified and excited by TG, cement, and composite exciter. The synergistic effect of the three components made the titanium-extracted residual slag-based cementitious material system show good reaction effects. In the initial stage of the reaction, lime, and sodium sulfate in the composite exciter enter the solution, rapidly increasing the PH value of the environment and providing active excitation conditions for TRS. At the initial stage, the alkaline environment formed by the dissolution of the composite activator and cement destroyed the glassy structure in the TRS [29], and constantly released Ca^{2+}, SO_4^{2+}, OH^- and CO_3^{2-}. This causes the silica tetrahedron and the more active aluminum tetrahedron in the TRS to undergo depolymerization reaction and fracture [30]. Under the alkaline solution environment, the depolymerized tetrahedra rebond with Ca^{2+}, Si^{2+}, and Al^{3+} in the solution to produce C-S-H gels and a small amount of C-A-H gels [31], which enhances the gelling properties. At the same time, the Al^{3+} released by depolymerization gradually increases the concentration of $[AlO]^{2-}$ in the solution and reacts with Ca^{2+} and SO_4^{2-} to form ettringite nuclei. The ettringite nuclei continue to develop and precipitate [32,33], and the strength of backfill continues to increase. At the same time, Na^+, Mg^{2+}, and Si^{4+} in the solution also participate in the hydration reaction to produce the calcite-like phase. From the products in the graphs, this process synchronized with the generation of calcium carbonate and potassium feldspar ($K_2O \cdot Al_2O_3 \cdot 6SiO_2$) and so on to gradually improve the strength of the specimens. With the increase in the curing time, the reaction gradually slows down, the structure becomes denser and the strength gradually increases. Each hydration reaction process is shown in Figure 15.
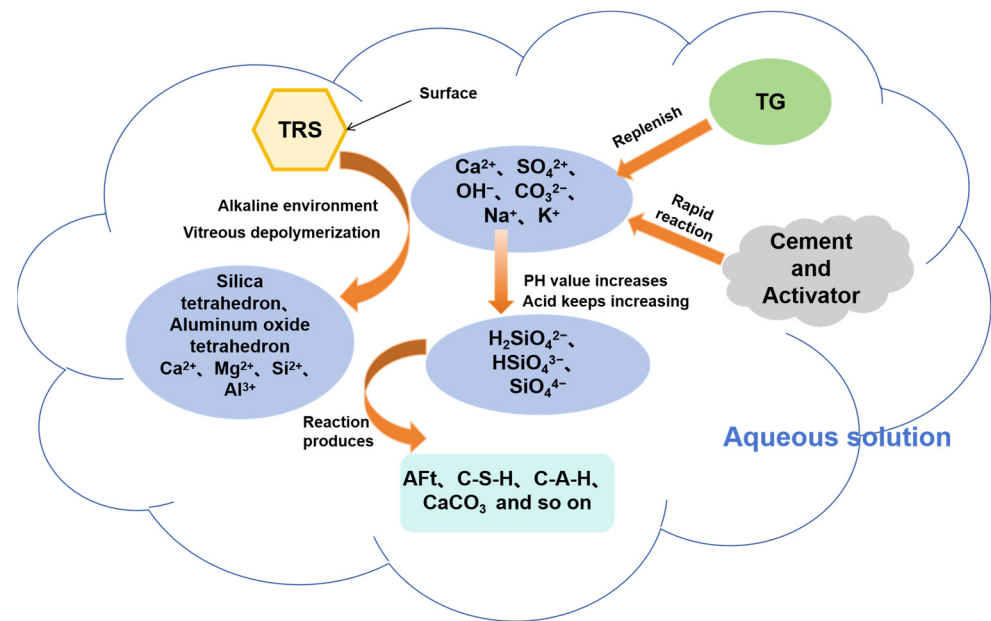
Figure 15. Schematic of the hydration reaction of titanium-extracted residual slag-based composite cementitious materials.

4.2.2. Microstructure and Strength Mechanisms

The microstructure of the backfill was observed by SEM. Figure 16 shows the micromorphology of backfill during hydration at different curing ages. As shown in Figure 16a, after 3 days of hydration, short columnar ettringite (Point A), calcium carbonate (Point B), and other products were distributed in the tailings void. From local magnification, it can be seen that the ettringite crystal is short and relatively sparse at this time, and the gel-like network type C-S-H (Point C) is distributed under the ettringite. In the backfill, due to the low OH^- in the initial stage of the hydration reaction, the pH value is low, and only part of the hydration products are produced. The source of this part of the product is the hydration reaction of cement, and a small amount of TRS vitreous depolymerization to form ettringite and calcium silicate hydrate, which provide strength for the early backfill.

As can be seen from Figure 16b, at the curing age of 14d, a large number of columnar ettringites appear in staggered nucleation distribution, constantly reaching into the space between tailings particles. From the local magnification, it can be seen that at this time, the growing columnar ettringite crystals are mostly attached to the TG, indicating that the TG participates in the formation of ettringite in this process. At the same time, gel-like C-S-H accumulates continuously with the prolongation of curing time, gradually wrapping tailings and ettringite into a whole [34]. When the pH value of the solution increased, the silicon (aluminum) oxygen tetrahedron in TRS quickly dissociated into the solution, and the oligosilicate ions and hydrolyzed ions in the aluminate ion solution quickly reacted to form C-S-H gel and ettringite, making the entire backfill structure relatively denser in the early stage [35].

It can be seen from Figure 16c that at the curing age of 28d, there are no obvious pores between the tailings particles inside the backfill, and the inside of the backfill is filled with hydration products. It can be seen from local magnification that the ettringite crystals at this time are fully developed, changing from needle-shaped to rod-shaped and interlacing with each other to connect the tailings particles into a whole. The C-S-H morphology develops from a sparse network structure to a dense layer structure and forms a large number of short columnar protrusions. The porosity is significantly reduced, the backfill is continuously densified, and the macroscopic performance is that the compressive strength of the backfill increases significantly.

In general, the titanium-extracted residual slag-based composite cementitious material has the characteristics of early strength and can reach more than 40% of the final 28d strength at 7 days. It is characterized by rapid development of strength in the early stage and high strength in the late stage, which can effectively reduce the cost of mine filling.
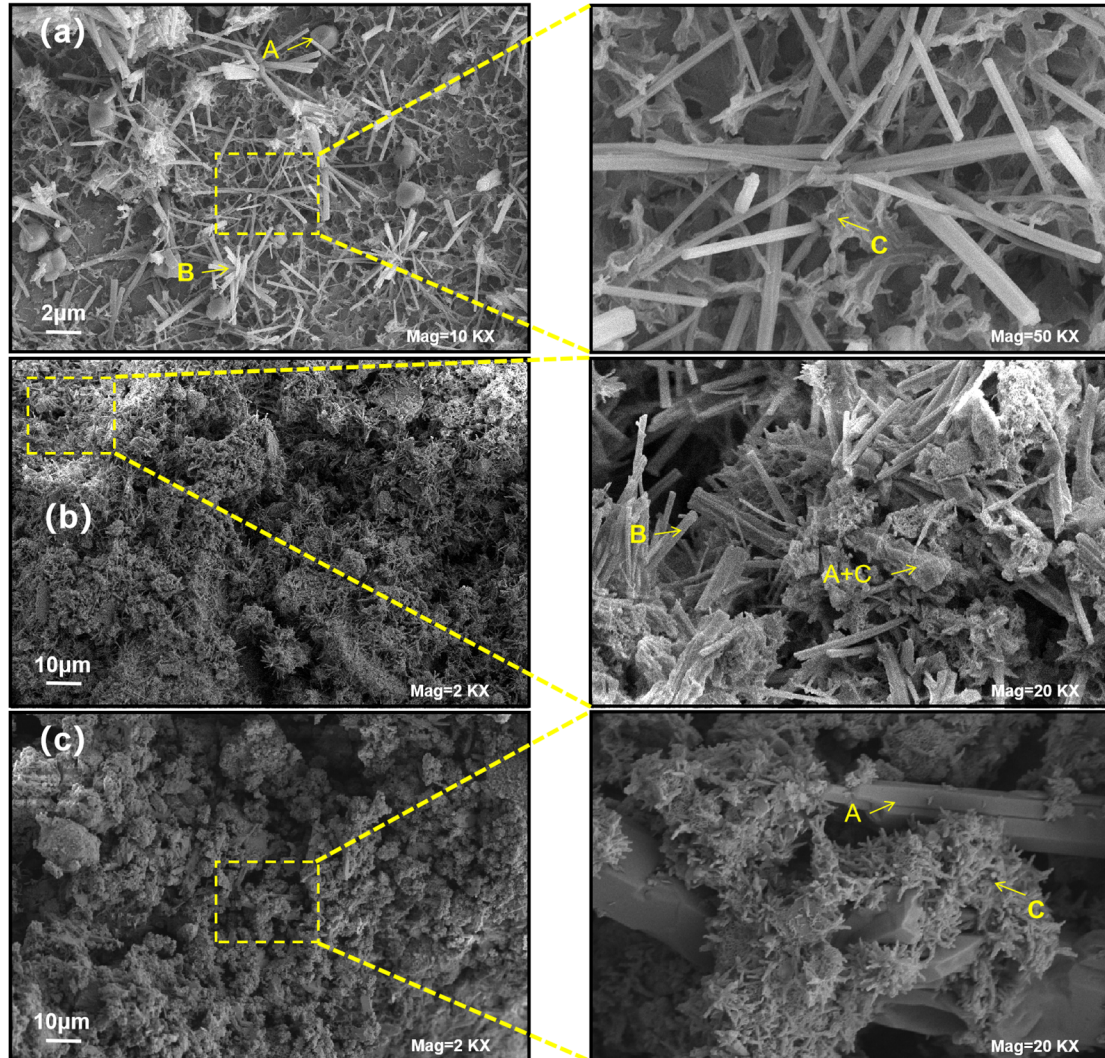

Figure 16. Micromorphology at each curing age (**a**) 3d; (**b**) 7d; (**c**) 28d.

5. Conclusions

The strength model of backfill at each age was analyzed by using Design-Expert to Design the mixing test, and the interaction and influence effect of various materials on the strength was analyzed. The sensitivity to the 3d strength of backfill was ranked in the order of composite activator > TG > TRS > cement, and the sensitivity to the strength of backfill at 7d and 28d was ranked as follows: Compound activator > cement > TRS > TG.

Through the combined action of TG, cement, and compound activator, the hydration activity of TRS was greatly improved, and the optimal ratio of the titanium-extracted residual slag-based composite cementitious material was TRS 55%, TG 25%, cement 17%, and compound activator 3%.

The hydration products of the titanium-extracted residual slag-based composite cementitious materials are mainly ettringite and C-S-H gel. In the early stage of the hydration reaction, the internal structure of the backfill is loose, and the hydration products are less, resulting in a relatively low backfill in the early stage. With the progress of the hydration reaction, ettringite gradually nucleates and intergrows with each other, C-S-H gel gradually

increases to cover tailing particles and ettringite, and the pores between tailing particles are gradually filled. When the pores are filled, the overall strength of the backfill reaches its maximum.

The strength of 3d, 7d, 14d, and 28d all-tailings cemented backfill prepared by the titanium-extracted residual slag-based composite cementitious material at 72% concentration, and 1:4 cement-sand ratio can reach 0.63 MPa, 2.11 MPa, 3.52 MPa, and 4.83 MPa. The titanium-extracted residual slag-based composite cementitious material solid waste accounted for up to 80%, the material cost is low, it does not easily absorb water and plate, its early strength performance is excellent, and it has good practical application value.

Author Contributions: Conceptualization, A.L. and J.L.; methodology, A.L.; software, M.L.; validation, J.L. and J.H.; formal analysis, A.L.; investigation, A.L.; resources, M.L.; data curation, A.L.; writing—original draft preparation, A.L.; writing—review and editing, J.L.; visualization, A.L.; supervision, M.L. and J.H.; project administration, J.X. and K.Z.; funding acquisition, J.L. All authors have read and agreed to the published version of the manuscript.

Data Availability Statement: The data presented in this study are available on request from the corresponding author. The data are not publicly available because the data in the research paper involves the confidentiality policy of the laboratory.

Conflicts of Interest: The co-authors Jianzhang Hao, Jiye Xu, and Ming Li are employees of the Pangang group, but the paper reflects the views of the scientists and not the company. The remaining authors declare that the research was conducted in the absence of any commercial or financial relationships that could be construed as a potential conflict of interest.

References

1. Kesimal, A.; Yilmaz, E.; Ercikdi, B.; Alp, I.; Deveci, H. Effect of properties of tailings and binder on the short-and long-term strength and stability of cemented paste backfill. *Mater. Lett.* **2005**, *59*, 3703–3709. [CrossRef]
2. Sun, K.; Fall, M. Response surface methodology-based characterization and optimization of fiber reinforced cemented tailings backfill with Slag. *Int. J. Min. Reclam. Environ.* **2023**, *37*, 735–759. [CrossRef]
3. Fall, M.; Célestin, J.; Pokharel, M.; Touré, M. A contribution to understanding the effects of curing temperature on the mechanical properties of mine cemented tailings backfill. *Eng. Geol.* **2010**, *114*, 397–413. [CrossRef]
4. Cao, H.; Gao, Q.; Zhang, X.; Guo, B. Research Progress and Development Direction of Filling Cementing Materials for Filling Mining in Iron Mines of China. *Gels* **2022**, *8*, 192. [CrossRef] [PubMed]
5. Shao, X.; Xu, B.; Tang, R.; Liu, L.; Fang, Z.; Tian, C.; Ning, J.; Li, L. Preparation and properties of a decarbonized coal gasification slag–fly ash filling material. *Environ. Sci. Pollut. Res.* **2023**, *30*, 45015–45028. [CrossRef] [PubMed]
6. Xue, G.; Yilmaz, E.; Wang, Y. Progress and prospects of mining with backfill in metal mines in China. *Int. J. Miner. Metall. Mater.* **2023**, *30*, 1455–1473. [CrossRef]
7. Zhang, S.; Wu, B.; Ren, Y.; Wu, Z.; Li, Q.; Li, K.; Zhang, M.; Yu, J.; Liu, J.; Ni, W. The Preparation Process and Hydration Mechanism of Steel Slag-Based Ultra-Fine Tailing Cementitious Filler. *Gels* **2023**, *9*, 82. [CrossRef] [PubMed]
8. Liu, W.; Chen, X.; Li, W.; Yu, Y.; Yan, K. Environmental assessment, management and utilization of red mud in China. *J. Clean. Prod.* **2014**, *84*, 606–610. [CrossRef]
9. Ren, C.; Li, K.; Wang, Y.; Li, Y.; Tong, J.; Cai, J. Preparation and Hydration Mechanisms of Low Carbon Ferrochrome Slag-Granulated Blast Furnace Slag Composite Cementitious Materials. *Materials* **2023**, *16*, 2385. [CrossRef] [PubMed]
10. Xu, Z.; Ma, Y.; Wang, J.; Shen, X. Preparation and Hydration Properties of Steel Slag-Based Composite Cementitious Materials with High Strength. *Materials* **2023**, *16*, 2764. [CrossRef] [PubMed]
11. Tang, S.; Peng, T.; Sun, H.; Ding, W.; Luo, L.; You, H.; Yao, X. Influences of Friedel's Salt Produced by CaO-Activated Titanium-Extracted Tailing Slag on Chloride Binding. *Materials* **2023**, *16*, 2843. [CrossRef] [PubMed]
12. Jing, J.; Tang, S.; Peng, T.; Sun, H.; Ding, W.; Luo, L.; You, H.; Yao, X. Recent Progress in Electric Furnace Titanium Slag Processing and Utilization: A Review. *Crystals* **2022**, *12*, 958. [CrossRef]
13. Li, J.; Li, A.; Hao, J.; Xu, J.; Zhang, L. Experimental study on the ratio between Ti-bearing blast furnace slag-iron-based full tailing sand and cement in cementitious filling. *J. Min. Sci. Technol.* **2023**, *8*, 838–846. (In Chinese)
14. Tang, S.; Peng, T.; Sun, H.; Ding, W.; Luo, L. Influencing Mechanism of Titanium-Extracted Tailing Slag on the Strength of CaO Steel Slag Hardened Paste. *Materials* **2023**, *16*, 937. [CrossRef] [PubMed]
15. Liao, G.Y. *Research on Proportional Optimization and Gelation Mechanism of Yellow Phosphorus Slag Filling*; Central South University: Changsha, China, 2009.

16. Ren, C.; Li, K.; Ni, W.; Zhang, S. Preparation of Mine Filling Material from Steel Slag Mud. *Ann. Chim. Sci. Mater.* **2019**, *43*, 217–224. [CrossRef]

17. Zhang, F.W. Investigations on Solidified Characteristics and Mechanism of Slag Cementitious Materials in Mine Filling. Ph.D. Thesis, Wuhan University, Wuhan, China, 2009. (In Chinese).

18. Lan, W.T.; Wu, A.X.; Yu, P. Development of a new controlled low strength filling material from the activation of copper slag: Influencing factors and mechanism analysis. *J. Clean. Prod.* **2020**, *246*, 119060. [CrossRef]

19. Zhang, J.Q.; Yang, K.; He, X.; Wei, Z.; Zhao, X.; Fang, J. Experimental Study on Strength Development and Engineering Performance of Coal-Based Solid Waste Paste Filling Material. *Metals* **2022**, *12*, 1155. [CrossRef]

20. El-Didamony, H.; Hafez, A.I.; Mohammed, M.S.; Sabry, R. Prepared and properties of filled and pozzolanic-filled cement from marble dust waste and granulated slag. *J. Therm. Anal. Calorim.* **2020**, *139*, 839–847. [CrossRef]

21. The General Administration of Quality Supervision, Inspection and Quarantine of the People's Republic of China, the Standardization Administration of China. *GB/T 18046-2017*; Ground Granulated Blast Furnace Slag Used for Cement, Mortar and Concrete. China Building Materials Federation: Beijing, China, 2018.

22. *GB/T51450-2022*; Metal and Non-Metal Mine Filling Engineering Technical Standard. Ministry of Housing and Urban-Rural Development: Beijing, China, 2022.

23. De Carvalho, J.M.F.; Defaveri, K.; Mendes, J.C.; Schmidt, W.; Kuehne, H.C.; Peixoto, R.A.F. Influence of particle size-designed recycled mineral admixtures on the properties of cement-based composites. *Constr. Build. Mater.* **2021**, *272*, 121640. [CrossRef]

24. Sanderson, R.A.; Cann, G.M.; Provis, J.L.; Ukpata, J.O.; Basheer, P.A.M.; Black, L.; Wang, P.Z.; Trettin, R.; Rudert, V.; Adam, T. The effect of blast-furnace slag particle size on the hydration of slag–Portland cement grouts at elevated temperatures. *Adv. Cem. Res.* **2018**, *30*, 337–344. [CrossRef]

25. Murgier, S.; Zanni, H.; Gouvenot, D. Blast furnace slag cement: A 29Si and 27Al NMR study. *Comptes Rendus Chim.* **2004**, *7*, 389–394. [CrossRef]

26. Li, Y.; Liu, X.; Sun, H.; Cang, D. Mechanism of phase separation in BFS (blast furnace slag) glass phase. *Sci. China Technol. Sci.* **2011**, *54*, 105–109. [CrossRef]

27. Ganesh Babu, K.; Kumar, V.S.R. Efficiency of GGBS in concrete. *Cem. Concr. Res.* **2000**, *30*, 1031–1036. [CrossRef]

28. Yong-ping, A.I.; Xie, S.-K. Hydration Mechanism of Gypsum–Slag Gel Materials. *J. Mater. Civ. Eng.* **2020**, *32*, 04019326. [CrossRef]

29. Tang, C.; Mu, X.; Ni, W.; Xu, D.; Li, K. Study on Effects of Refining Slag on Properties and Hydration of Cemented Solid Waste-Based Backfill. *Materials* **2022**, *15*, 8338. [CrossRef] [PubMed]

30. Liu, Z.; Ni, W.; Li, Y.; Ba, H.; Li, N.; Ju, Y.; Zhao, B.; Jia, G.; Hu, W. The mechanism of hydration reaction of granulated blast furnace slag-steel slag-refining slag-desulfurization gypsum-based clinker-free cementitious materials. *J. Build. Eng.* **2021**, *44*, 103289. [CrossRef]

31. Dong, Y.; Feng, C.; Zhao, Q.; Liang, X. Study on the Structure of C-S-H Gels of Slag–Cement Hardened Paste by ^{29}Si, ^{27}Al MAS NMR. *Appl. Magn. Reson.* **2019**, *50*, 1345–1357. [CrossRef]

32. Wang, Z.; Wang, Z.; Xia, H.; Wang, H. Analysis of hydration mechanism and microstructure of composite cementitious materials for filling mining. *J. Wuhan Univ. Technol. Mater. Sci. Ed.* **2017**, *32*, 910–913. [CrossRef]

33. Zhao, X.; Yang, K.; He, X.; Wei, Z.; Zhang, J. Study on proportioning experiment and performance of solid waste for underground backfilling. *Mater. Today Commun.* **2022**, *32*, 103863. [CrossRef]

34. Xu, W.; Tian, M.; Li, Q. Time-dependent rheological properties and mechanical performance of fresh cemented tailings backfill containing flocculants. *Miner. Eng.* **2020**, *145*, 106064. [CrossRef]

35. Zhu, M.; Xie, G.; Liu, L.; Wang, R.; Ruan, S.; Yang, P.; Fang, Z. Strengthening mechanism of granulated blast-furnace slag on the uniaxial compressive strength of modified magnesium slag-based cemented backfilling material. *Process Saf. Environ. Prot.* **2023**, *174*, 722–733. [CrossRef]